Soft Matter

ARTICLE TYPE

Cite this: DOI: 00.0000/xxxxxxxxxx

In-situ aggregation and early states of gelation of gold nanoparticle dispersions†

Florian Schulz,*[a,b] Avni Jain,[c‡] Francesco Dallari,[c§] Verena Markmann,[c¶] and Felix Lehmkühler[b,c]

Received Date
Accepted Date

DOI: 00.0000/xxxxxxxxxx

The aggregation and onset of gelation of PEGylated gold nanoparticles dispersed in a glycerol-water mixture is studied by small-angle X-ray scattering and X-ray photon correlation spectroscopy. Tracking structural dynamics with sub-ms time resolution over a total experimental time of 8 hours corresponding to a time windows larger than 10^8 Brownian times and varying the temperature between 298 K and 266 K we can identify three regimes. First, while cooling to 275 K the particles show Brownian motion that slows down due to the increasing viscosity. Second, upon further cooling the static structure changes significantly, indicated by a broad structure factor peak. We attribute this to the formation of aggregates while the dynamics are still dominated by single-particle diffusion. Finally, the relaxation functions become more and more stretched accompanied by an increased slow down of the dynamics. At the same time the structure changes continuously indicating the onset of gelation. Our observations further suggest that the colloidal aggregation and gelation is characterized first by structural changes with a subsequent slowing down of the systems dynamics. The analysis also reveals that the details of the gelation process and the gel structure strongly depend on the thickness of the PEG-coating of the gold nanoparticles.

1 Introduction

Soft matter systems are known to show a rich phase behavior[1,2]. In particular colloidal dispersions, i.e. solid particles of nm to μm size dispersed in a liquid, can occur in different phases and states, such as liquid, crystalline and amorphous solids. Understanding the structure and dynamics through the phase diagram, especially during the transition between two states, is a main route of current soft matter and nanoscience research. The formation of colloidal gel states in particular is a complex subject of long-standing scrutiny[3–5].

Polymer-stabilized gold nanoparticles can be considered a relatively new class of materials that is explored for applications ranging from energy conversion to bio-nanotechnology and nanomedicine among others[6–8]. For processing, stability and safe application it is crucial to understand the phase behavior of these materials. Besides self-assembly into supercrystals[9], these particles show formation of a colloidal gel, which enables the application as a model system for studying gelation processes with a temporal and spatial resolution that can hardly be achieved experimentally on an atomic scale.

In general, experiment and theory have reported different gelation mechanisms, the most common ones are gelation via spinodal decomposition[4,5,10–12], and percolation[13–15], or combinations of both[16–18]. Typically, colloidal gels are formed with attractive particles, or e.g., after transitions from repulsion to attraction[12,19–22]. Thanks to the attractive interaction, the particles may form amorphous network structures which is characterized structurally by formation of aggregates accompanied by a slow down of the structural dynamics by orders of magnitude[15,18,23–29].

Despite of decades of research on aggregation and gelation our understanding of the structure and dynamics within these processes is still largely incomplete, in particular from an experimental point of view[4,10,30]. To track these processes, X-ray photon correlation spectroscopy at modern X-ray light sources allows both the necessary spatial resolution covering nm length scales as

[a] Institute of Nanostructure and Solid State Physics, University of Hamburg, Luruper Chaussee 149, 22761 Hamburg, Germany
[b] The Hamburg Centre for Ultrafast Imaging, Luruper Chaussee 149, 22761 Hamburg, Germany.
[c] Deutsches Elektronen-Synchrotron DESY, Notkestr. 85, 22607 Hamburg, Germany. E-Mail: felix.lehmkuehler@desy.de

† Electronic Supplementary Information (ESI) available: [details of any supplementary information available should be included here]. See DOI: 10.1039/cXsm00000x/

‡ Present address: Blue Yonder GmbH, Oberbaumbrücke 1, 20457 Hamburg, Germany.
§ Present address: University of Padua, Department of Physics and Astronomy, Via Marzolo 8, 35121 Padova, Italy.
¶ Present address: Department of Physics, Technical University of Denmark, Kgs. Lyngby 2800, Denmark.

well as time resolution of sub-ms to probe the dynamics of the particles in real time[31]. XPCS is frequently used to study soft matter systems, e.g., obtaining structural and dynamical information of diffusion and hydrodynamic interactions on microsecond timescales[32–37], glasses and glass transitions[38–45], and colloidal gelation[43,46–53]. Recently, we have used XPCS to study the gelation of colloidal gold particles grafted with polyethylene (PEG) based ligands and dispersed in a water-glycerol mixture[29,54]. With ligands of 5 kDa weight, we found a three-step gelation process at 272 K studying structure and dynamics over approximately 3 hours experimental time.

Here, we extend our recent work on the structure and dynamics of PEGylated gold nanoparticles dispersed in a glycerol-water mixture. We focus on shorter PEG ligands of 2 kDa weight, but the same volume fraction. The structure and dynamics of the dispersion is tracked by small-angle x-ray scattering (SAXS) and XPCS over a total experimental time of 8 hours, with a time resolution of about 10^{-4} s. In contrast to the previous study with longer PEG ligands, the particles form aggregates before the gelation sets in at lower temperatures and after longer waiting times. Cooling the sample from 298 K and 266 K we can identify three regimes: (I) Brownian motion of non-interacting particles for $T \geq 275$ K, (II) formation of aggregates, but accompanied by diffusive particle dynamics, and (III) onset of gelation at 266 K characterized by a slowing down of the structural dynamics and an ongoing formation of larger structural units. Our results demonstrate that a small difference in a structural feature, here the thickness of the PEG-coating, can completely change the aggregation and gelation mechanisms.

2 Experimental

2.1 Sample details

The sample consisted of gold nanoparticles (AuNP) coated with α-methoxypoly(ethylene glycol)-ω-(11-mercaptoundecanoate) (PEGMUA, 2 kDa) dispersed in a mixed solvent of glycerol and water (70:30 v/v). The synthesis of these particles has been reported previously[55,56]. The radius of the gold nanoparticles was about 6.1 nm with a size dispersity of less than 10%. The ligand shell thickness is about 8 nm in pure water[57]. The particles were concentrated to approximately 7 vol.% , calculated with an particle concentration of 10 μM (determined with UV/vis spectroscopy) and a thickness of the PEG-shell of 8 nm. Dispersions of such particles at similar volume fractions but with longer ligands (5kDa PEGMUA, shell thickness approx. 12 nm) have been found to form colloidal gels at temperatures around $T_{\mathrm{gel}} \sim 280$ K[29,54]. For $T < T_{\mathrm{gel}}$, the particle interactions become attractive, promoting network formation and thus gelation.

2.2 Coherent X-ray scattering experiments

The XPCS experiments have been performed at beamlines CHX (11-ID) of NSLS-II (Upton, NY, USA) and P10 of PETRA III at DESY (Hamburg, Germany). At CHX, we used a beam energy of 9.6 keV and a beamsize of 10 μm $\times$ 10 μm. The detector (Eiger500k) was placed 10 m downstream the sample. At P10, the ultra small-angle X-ray scattering (USAXS) geometry was used. The detector (Eiger500k) is placed 21.2 m downstream the sample position. In our experiment, the beam energy was 8.1 keV and its size was set to 100 μm $\times$ 100 μm using slits. In both experiments, the samples were filled to borosilicate capillaries (Hilgenberg GmbH) of 1 mm inner diameter and 10 μm wall thickness. The capillaries were placed into temperature-controllable sample holders available at both beamlines. The sample environments were evacuated afterwards to reduce the scattering background. Series of several thousand speckle patterns were measured at the maximum frame rate of 9 kHz of the Eiger500k detector in both experiments. Owing to the different geometries in both experiments, the accessible q-range was different. At CHX we could cover about 0.012 nm^{-1} to 0.32 nm^{-1}, while at P10 the q-range was between 0.006 nm^{-1} and 0.12 nm^{-1} for the $I(q)$.

Data from the experiment at CHX is labeled run 1, while run 2 refers to data from P10. In run 1 we measured the XPCS series starting at 298 K. Subsequently, we reduced the temperature in several steps. At each temperature, several XPCS runs were measured at different sample spots and different attenuator settings to check for radiation-induced effects on structure and dynamics (see ESI). The first XPCS run was started directly after the target temperature was achieved. Below 280 K, which was found as gelation temperature for similar samples with 5 kDa ligands, we chose a step size of $\Delta T = 1$ K, down to 266 K for run 1. In both experiments, we found an onset temperature for structural changes (see discussion below) of $T_0 = 272$ K. When T_0 has been reached, we set $t_w = 0$ s and label the following measurements with both temperature and t_w. We included waiting times to determine a slowing down and change of structure as observed during gelation[29,54]. In run 2, the temperature was reduced in several steps starting from $T = 293$ K. Here, at the lowest temperature studied ($T_0 = 272$ K) series of speckle patterns were measured continuously. Due to the larger beamsize in run 2, sample spots had to be measured several times with at least 600 s between two measurements. The total experimental time were $t_{1,\max} = 28600$ s (run 1) and $t_{2,\max} = 11400$ s (run 2), respectively. T_0 was reached at after about 5200 s for run 2 and at about 17000 s for run 1, thus we obtained the maximum of t_w as $t_{w,1,\max} = 11514$ s and $t_{w,2,\max} = 6544$ s. In this way we covered a dynamic range of the experiment of $> 10^8 \tau_B$, with τ_B the Brownian time of the particles.

2.3 XPCS

In XPCS experiments, sample dynamics are obtained by autocorrelations of the speckle patterns, i.e. diffraction patterns in a coherent X-ray scattering experiment, given by[31,58–60]

$$g_2(q,t) = \frac{\langle I(q,t')I(q,t'+t)\rangle_{t'}}{\langle I(q,t')\rangle_{t'}^2}. \quad (1)$$

$I(q,t')$ is the intensity at time t' and the modulus of the wave vector transfer $q \equiv |\mathbf{q}| = 4\pi \sin(\theta/2)/\lambda$, with wavelength λ and scattering angle θ. The g_2 function is related to the intermediate scattering function $f(q,t)$ and can be modelled in many cases by

a Kohlrausch-Williams-Watts (KWW) expression

$$g_2(q,t) = 1 + \beta |f(q,t)|^2 = 1 + \beta \exp(-2(t/\tau)^\gamma). \quad (2)$$

Here, β is the speckle contrast defined by coherence properties of the x-ray beam and setup parameters, τ the characteristic relaxation time and γ the KWW exponent. The q-dependence of $\tau \propto q^{-p}$ and the KWW exponent γ define the type of dynamics, e.g., diffusion results in $p = 2$ and $\gamma = 1$. Thus, for diffusive samples, the intermediate scattering function can be described as

$$f(q,t) = \exp(-q^2 D(q) t), \quad (3)$$

where $D(q)$ denotes a q-dependent diffusivity.

3 Results

Correlation functions g_2 are shown for run 2 in Fig. 1 measured at $q = 0.045$ nm^{-1}. The q-dependence of g_2-functions measured at different t_w is shown in the ESI. In the left panel in Fig. 1 the data is taken at different temperatures at the start of the whole time series. With decreasing temperature, the correlation functions decay at longer times t due to the increase of viscosity. The two datasets at $T = 272$ K represent the first (star symbols) and last (right-pointing triangles) measurement at this temperature. To track the evolution of g_2 at $T = 272$ K, correlation functions are shown in the right panel for different experimental times t_w. This suggests a slowing down of dynamics with t_w. In order to obtain the relaxation time τ and the KWW exponent γ, Eq. 2 has been fitted to the correlation functions. The speckle contrast β was allowed to vary around the value obtained from measurements of a static sample of 0.10 ± 0.01.

Relaxation times from both runs are shown in Fig. 2. Here, τ measured at $q = 0.045$ nm^{-1} is plotted as a function of T. In case of diffusion, the q-dependence of τ is $1/\tau = Dq^2$, with the Stokes-Einstein diffusion constant

$$D = \frac{k_B T}{6\pi\eta(T) r}. \quad (4)$$

Here, η denotes the viscosity of the solvent and r the particle radius. For $T > 272$ K the relaxation time follows the expectation of the Stokes-Einstein relation with a particle radius of 14 nm in excellent agreement with previous studies using different methods (dynamic light scattering, structure factor analysis, polymer physics models) to estimate the thickness of the ligand shell[57]. The viscosity η was calculated using the temperature-dependence of water-glycerol mixtures from literature[61]. Above T_0 the measured relaxation times follow the model for both runs, indicating free diffusion of the particles. This confirms that negligible amounts of aggregates are present above the gelation-temperature in the highly concentrated colloidal dispersion. Below approximately 272 K, the relaxation time slows down up to several 100 ms, thus, more than one order of magnitude slower than for diffusion. While we continued cooling step-wise in run 1, the sample was kept at 272 K and its aging was measured over several hours in run 2. Thus, the data from run 1 represents a combination of cooling and aging of the dynamics below 272 K, while for run 2 the aging was studied in detail at the onset temperature of slowing down of 272 K. The temperature-dependence of τ can be described by Arrhenius laws $\tau = \tau_0 \exp\left(\frac{E_a}{k_B T}\right)$. For $T > 272$ K where the data follows the viscosity model, we find an activation energy of $E_a^{\text{high}} = 44.5$ kJ/mol which describes the change of viscosity. For lower temperatures, we found $E_a^{\text{low}} = 156$ kJ/mol for the data taken shortly after the goal temperature was reached (filled symbols). As here the relaxation times are subject to aging we found a larger energy of $E_a^{\text{wait}} = 268$ kJ/mol for data taken after 1000 s waiting time (see ESI for details). These energies are slightly larger than observed in other colloidal systems undergoing aggregation[62–64]. The evolution of τ and the KWW exponent γ with experimental time t_w is further evaluated in the ESI. Typically, we found $\gamma \approx 0.9$ - 1 in both runs which is typically found for such particles with long ligands undergoing diffuse motion[29]. At 266 K studied in run 1 we find a decreasing exponent as function of t_w that coincides with the abrupt slowing down of the dynamics. Such stretched correlation functions have been reported in different studies on glass and gel transitions as a fingerprint of the solidification[29,39,42,43,65–67] so that we associate it to the onset of macroscopic gel formation.

As we could only access the dynamics for very few q-values in run 1 we could not model the q-dependence of the dynamics. Thus, there is only a limited information on the change of dynamics with t_w for run 1. Thanks to the lower q-range accessible in run 2, the g_2-functions could be further analyzed for different q-values. We found a q-dependence of $1/\tau \propto q^2$ indicating diffusive dynamics for all t_w, in particular at 272 K. This enabled us to calculate an effective diffusion constant $D(q)$ shown in Fig. 3 for both different temperature and t_w of run 2.

For $T > 272$ K the diffusion constant follows the Stokes-Einstein relation as discussed above for the relaxation time. In contrast, at $T = 272$ K the diffusion constant continues to decrease with waiting over several 1000 s following a power law $D \propto t_w^{-2}$. However, different from previous studies on the same particles with longer ligands[29], we do not see further indications of gelation. In particular, the dynamics remain (sub-)diffusive with $p = 2$, and the KWW exponent γ in the range of 0.8 to 1 (see ESI). This is remarkable, because a slightly smaller thickness of the PEG-ligand-shell (about 4 nm difference) seems to result in a significantly differing gelation behaviour, when all other parameters (AuNP core radius, volume fraction, glycerol content, temperature) are similar.

To connect the dynamics with structural properties, we take a closer look on the structure factors $S(q)$. These where obtained by normalizing the intensity to the equilibrium intensity at room temperature as $S(q) = I(q,T)/I(q,T_R)$ with $T_R = 293$ K, see Fig. 4 a. Intensities $I(q)$ are shown in the ESI. Note that $I(q,T_R)$ resembles the form factor of the particles well in the studied q-range, in particular the dominant contribution from the gold core, and was therefore chosen as effective form factor (see ESI for details). Here, we also show the data for run 2 which were measured for smaller q values. This allows us to detect the evolution of the strong signal between 10^{-2} nm^{-1} and 10^{-1} nm^{-1} after reaching 272 K. Cooling from 298 K to 274 K, the $S(q)$ remains unchanged and suggests no difference from form factor of spherical particles at low q. Between 273 K and 271 K an increase below 0.1 nm^{-1}

is found. Further cooling towards 266 K leads to strong increase of $S(q)$ at low q which is typically associated with appearance of agglomerates. This is accompanied by a decrease around 0.2 nm^{-1}. Noteably, instead of an upturn for $q \to 0$ that is suggested from the $I(q)$, a broad peak is found whose peak position stays constant around $q_{peak} \approx 0.0105$ nm^{-1}, corresponding to a length scale of $2\pi/q_{peak} \approx 600$ nm. However, thanks to the broad peak it does not reflect a particular correlation length in the systems but rather a wide distribution of length scales with full width at half maximum of 1200 nm.

We further quantified this structural change by calculating the Ornstein-Zernike correlation length ξ and the scattering invariant Q. The access to the small-angle regime allows the calculation of ξ in the framework of the Ornstein-Zernike theory[68]. At low q, the intensity can be approximated by

$$I(q) = \frac{I_0}{1+\xi^2 q^2}. \quad (5)$$

Similar to our previous study on longer PEG ligands[29], we calculated ξ for run 2, shown in Fig. 4 b. As we did not have access to such small q in run 1, ξ cannot be calculated with a comparable reliability. We find much lower values as observed for 5k PEG ligands where ξ increased above 1000 nm in the colloidal gel. For small t_w, ξ is close to the radius of the gold cores assuming no particle correlation beyond the single particle. With increasing t_w and at lower T the correlation length increases above 30 nm. This supports the formation of aggregates rather than a network formation such as found for colloidal gels and in particular with 5k ligands.

The scattering invariant is given by[69–71]

$$Q = \int_{q_{min}}^{q_{max}} q^2 I(q) \mathrm{d}q. \quad (6)$$

As integration limits we chose $q_{min} = 10^{-2}$ nm^{-1} and $q_{max} = 10^{-1}$ nm^{-1}. This q-range could be covered in both experiments so that both data can be compared directly. The invariant is a constant when integrated over the whole q region, as it covers structural changes that result in contributions to $I(q)$ at different q-values. Consequently, we find a constant invariant using $q_{max} \geq 0.2$ nm^{-1} (see ESI). However, when studying a limited q-range, it can be used as a measure of structural changes at the corresponding length scales[72–74]. In Fig. 4 c the scattering invariant is shown for both runs. While cooling from room temperature the scattering invariant stays constant up to 275 K. With further cooling, it increases first moderately. For $T \leq T_0$ a strong increase is found with both cooling and waiting time. At the end of run 1 the scattering invariant has almost tripled compared to its initial value.

Finally, we analyze the correlation between structural and dynamical properties. To this end, the scattering invariant and the correlation length ξ are compared to the diffusion constants obtained by XPCS in Fig. 5. First, we can identify three different regimes from the left panel: (I) Cooling from room temperature to 275 K the scattering invariant does not vary while the diffusion constant decreases by a factor of 4 due to the increase of viscosity with cooling. (II) For 275 K $\geq T \geq$ 268 K the scattering invariant doubles its values. At the same time, the diffusion constant decreases only slightly. (III) At low temperatures and long waiting times, the scattering invariant increases and the relaxation time decreases continuously. These regimes can be transferred to the Ornstein-Zernike correlation length ξ (right panel). Here, in regime I we find a growth of ξ by about a factor of 2 that correlates with the decrease of D by a factor of approximately 6. Regime II is characterized by a reverse behaviour, i.e., ξ strongly grows while D decreases slightly, similar to the result found for the scattering invariant. Finally, regime III is dominated by a continuous grows of ξ, from about 50 nm towards 1000 nm. The continuous growth of ξ and the behaviour of the scattering invariant suggests the onset of gelation, e.g., we found $\xi > 1000$ nm for the gel phases formed by particles with longer ligands[29]. This is supported by further parameters, e.g., the KWW exponent that decreases in this regimes (see ESI).

4 Conclusion

We tracked the early states of gelation of PEGylated gold particles by means of XPCS. Compared to particles with longer ligands (5 kDa vs. 2 kDa)[29], the gelation takes place at lower temperatures and longer time scales. Below an onset temperature of 272 K, where particles with longer ligands in fact formed a gel within few 1000 s, we observe the formation of larger structural units with typical sizes of several 100 nm. While the structural change is much more prominent than observed in the gelation study with 5 kDa ligands, the dynamics stay diffusive. When staying at the gelation onset temperature (run 2) the diffusivity shows only a small reduction which would correspond to an effective particle radius of $r_\infty \approx 25$ nm, still resembling Brownian motion. This indicates that despite of the formation of larger structural units, the particles are still mobile within the aggregates and only slightly slowed down showing all indications of diffusive dynamics. Our conclusions are also supported by the study of the Ornstein-Zernike correlation length which grows from about 6 nm to 32 nm in this regime. This suggests the formation of aggregates in this run and not a network as found during colloidal gelation[29]. A comparison of relaxation times and KWW exponents for 2 kDa and 5 kDa ligands suggests that in fact we observe the onset of gelation in regime III, however, taking place at lower temperatures for shorter ligands and progressing a factor of 6 to 7 slower (see ESI). Notably, in biological matter a tendency to form aggregates is also found for particles with 2 kDa PEG ligands, whereas in that case the particles with longer ligands were stable[35].

PEG-coated gold nanoparticles are well-known for their excellent stability in a broad range of conditions[75]. As PEG is strongly hydrophilic, its hydration state is crucial for analyzing its properties. With the glycerol-water mixture used here, the amount of water molecules available for PEG is reduced. In previous studies we determined that about 230 water molecules can be bound per PEG2k molecule in a fully hydrated PEG-shell on AuNP[57,76]. Thus, the full hydration of the PEG-coated nanoparticles requires approximately 3.5 M of the available water. However, even without nanoparticles, all available water molecules would be bound to glycerol for the concentration used here[77], therefore, PEG and glycerol compete for the available water in the system. A pre-

ferred hydration of glycerol would result in attractive PEG-PEG interactions in this system, because the remaining water is not sufficient to fully hydrate the PEG coatings. In consequence the PEG-coated AuNP agglomerate. Note that a full thermodynamic analysis of the involved hydrogen bond networks with the three constituents water, glycerol and PEG is far from trivial and beyond the scope of this study.

Comparing structure and dynamics, we find three regimes of aggregation and gel formation. In regime I representing cooling from room temperature to 275 K the dynamics slow down due to the increased viscosity of the solvent. The structure remains mainly unchanged, no significant variation from $S(q) = 1$ with a slight growth of ξ and Brownian motion is measured. By further cooling to 268 K we find regime II, where the dynamics slow down slightly more than expected from the viscosity. At the same time a structure factor dominates the scattering pattern with a broad peak. This is expressed by a doubling of the scattering invariant and a tripling of ξ in this temperature regime. We interpret this as formation of aggregates with still mobile particles showing diffusive dynamics, but with slow aging. Compared to the study on 5k PEG ligands[29], about a factor of three less water is needed for 2k PEG considering the particle concentration, the larger number of water per PEG ligand, and different coating density. This may result in more PEG-PEG attractive interactions and entanglement leading to network formation and thus gelation for the 5k PEG ligands whereas for the 2k PEG ligands it results in agglomeration with very slow aging. Finally, in regime III corresponding to low temperatures and long waiting times, both the relaxation time, scattering invariant and ξ increase continuously. Moreover, the KWW exponent γ gets smaller, indicating a broadening of the distribution of relaxation times. While this observation is in line with an onset of gelation, it may also be interpreted as increased growth of agglomerates with broader size distribution. However, the data matches the results observed previously for longer ligands[29] where a gel was formed, taking place on much longer time scales. In conclusion, our results indicate that in the studied system of PEGylated gold particles dispersed in a water-glycerol mixture the processes of agglomeration and onset of gelation is highly dependent on the hydration state of the PEG ligands. It is governed first by structural changes – from single particles to larger agglomerates – before the dynamics slow down. Our data underline, that even small changes of nanoparticle geometry can strongly affect their gelation and agglomeration behavior, which in the case of plasmonic particles will also affect their optical response[78,79].

Author Contributions

Florian Schulz: Conceptualization (equal) Data curation (equal) Investigation (equal) Project administration (supporting) Resources (lead) Validation (equal) Writing - review & editing (equal)

Avni Jain: Conceptualization (equal) Data curation (equal) Formal analysis (equal) Investigation (equal) Methodology (equal) Project administration (supporting) Software (equal) Visualization (equal) Writing - review & editing (equal)

Francesco Dallari: Data curation (equal) Funding acquisition (equal) Investigation (equal) Software (equal) Validation (equal) Writing - review & editing (equal)

Verena Markmann: Data curation (equal) Investigation (equal) Validation (equal) Writing - review & editing (equal)

Felix Lehmkühler: Conceptualization (equal) Data curation (equal) Formal analysis (equal) Funding acquisition (lead) Investigation (equal) Methodology (equal) Project administration (equal) Software (equal) Supervision (equal) Visualization (equal) Writing - original draft (equal) Writing - review & editing (equal)

Conflicts of interest

There are no conflicts to declare.

Acknowledgements

The authors acknowledge DESY (Hamburg, Germany), a member of the Helmholtz Association HGF, for the provision of experimental facilities. Parts of this research were carried out at PETRA III. The authors thank Fabian Westermeier for assistance in using the P10 beamline and Wojciech Roseker for critical reading of the manuscript.

This research used beamline CHX (11-ID) of the National Synchrotron Light Source II, a U.S. Department of Energy (DOE) Office of Science User Facility operated for the DOE Office of Science by Brookhaven National Laboratory under Contract No. DE-SC0012704. We thank Yugang Zhang, Lutz Wiegart and Andrei Fluerasu for assistance.

This work was financially supported by DESY, a member of the Helmholtz Association (HGF), and by the Cluster of Excellence "Advanced Imaging of Matter" of the Deutsche Forschungsgemeinschaft (DFG) – EXC 2056 – project ID 390715994.

Notes and references

1 L. Berthier and G. Biroli, *Rev. Mod. Phys.*, 2011, **83**, 587–645.
2 G. L. Hunter and E. R. Weeks, *Rep. Progr. Phys.*, 2012, **75**, 066501.
3 V. Trappe and P. Sandkühler, *Curr. Opin. Colloid Interface Sci.*, 2004, **8**, 494–500.
4 E. Zaccarelli, *J. Phys.: Condens. Matter*, 2007, **19**, 323101.
5 C. P. Royall, M. A. Faers, S. L. Fussell and J. E. Hallett, *J. Phys.: Condens. Matter*, 2021, **33**, 453002.
6 R. Sardar, A. M. Funston, P. Mulvaney and R. W. Murray, *Langmuir*, 2009, **25**, 13840–13851.
7 M. I. Anik, N. Mahmud, A. Al Masud and M. Hasan, *Nano Select*, 2021, **3**, 792–828.
8 I. Hammami, N. M. Alabdallah, A. A. jomaa and M. kamoun, *J. King Saud Univ. Sci.*, 2021, **33**, 101560.
9 F. Schulz, I. Lokteva, W. J. Parak and F. Lehmkühler, *Part. Part. Syst. Char.*, 2021, **38**, 2100087.
10 M. E. Cates, M. Fuchs, K. Kroy, W. C. K. Poon and A. M. Puertas, *J. Phys.: Condens. Matter*, 2004, **16**, S4861–S4875.
11 S. Manley, H. M. Wyss, K. Miyazaki, J. C. Conrad, V. Trappe, L. J. Kaufman, D. R. Reichman and D. A. Weitz, *Phys Rev Lett*, 2005, **95**, 238302.

12 P. J. Lu, E. Zaccarelli, F. Ciulla, A. B. Schofield, F. Sciortino and D. A. Weitz, *Nature*, 2008, **453**, 499–503.
13 A. P. R. Eberle, N. J. Wagner and R. Castañeda-Priego, *Phys Rev Lett*, 2011, **106**, 105704.
14 M. Kohl, R. F. Capellmann, M. Laurati, S. U. Egelhaaf and M. Schmiedeberg, *Nat Commun*, 2016, **7**, 11817.
15 J. Rouwhorst, C. Ness, S. Stoyanov, A. Zaccone and P. Schall, *Nat. Commun.*, 2020, **11**, 3558.
16 H. Tsurusawa, M. Leocmach, J. Russo and H. Tanaka, *Sci. Adv.*, 2019, **5**, eaav6090.
17 S. Zhang, L. Zhang, M. Bouzid, D. Z. Rocklin, E. D. Gado and X. Mao, *Phys. Rev. Lett.*, 2019, **123**, 058001.
18 M. Tateno, T. Yanagishima and H. Tanaka, *J. Chem. Phys.*, 2022, **156**, 084904.
19 V. Trappe, V. Prasad, L. Cipelletti, P. N. Segre and D. A. Weitz, *Nature*, 2001, **411**, 772–775.
20 A. M. Puertas, M. Fuchs and M. E. Cates, *Phys. Rev. E*, 2003, **67**, 031406.
21 E. Zaccarelli and W. C. K. Poon, *Proc. Natl. Acad. Sci.*, 2009, **106**, 15203–15208.
22 L. Frenzel, F. Lehmkühler, I. Lokteva, S. Narayanan, M. Sprung and G. Grübel, *J. Phys. Chem. Lett.*, 2019, **10**, 5231–5236.
23 T. A. Witten and L. M. Sander, *Phys. Rev. Lett.*, 1981, **47**, 1400–1403.
24 D. A. Weitz and M. Oliveria, *Phys. Rev. Lett.*, 1984, **52**, 1433–1436.
25 R. C. Ball, D. A. Weitz, T. A. Witten and F. Leyvraz, *Phys. Rev. Lett.*, 1987, **58**, 274–277.
26 M. Y. Lin, H. M. Lindsay, D. A. Weitz, R. C. Ball, R. Klein and P. Meakin, *Nature*, 1989, **339**, 360–362.
27 Z. Wang, J. Nie, W. Qin, Q. Hu and B. Z. Tang, *Nat. Commun.*, 2016, **7**, 12033.
28 J. de Graaf, W. C. K. Poon, M. J. Haughey and M. Hermes, *Soft Matter*, 2019, **15**, 10–16.
29 A. Jain, F. Schulz, F. Dallari, V. Markmann, F. Westermeier, Y. Zhang, G. Grübel and F. Lehmkühler, *J. Chem. Phys.*, 2022, **157**, 184901.
30 Y. Jiang and R. Seto, *Nat. Commun.*, 2023, **14**, 2773.
31 F. Lehmkühler, W. Roseker and G. Grübel, *Appl. Sci.*, 2021, **11**, 6179.
32 F. Lehmkühler, F. Dallari, A. Jain, M. Sikorski, J. Möller, L. Frenzel, I. Lokteva, G. Mills, M. Walther, H. Sinn, F. Schulz, M. Dartsch, V. Markmann, R. Bean, Y. Kim, P. Vagovic, A. Madsen, A. P. Mancuso and G. Grübel, *Proc. Natl. Acad. Sci.*, 2020, **117**, 24110–24116.
33 F. Dallari, A. Jain, M. Sikorski, J. Möller, R. Bean, U. Boesenberg, L. Frenzel, C. Goy, J. Hallmann, Y. Kim, I. Lokteva, V. Markmann, G. Mills, A. Rodriguez-Fernandez, W. Roseker, M. Scholz, R. Shayduk, P. Vagovic, M. Walther, F. Westermeier, A. Madsen, A. P. Mancuso, G. Grübel and F. Lehmkühler, *IUCrJ*, 2021, **8**, 775–783.
34 M. Reiser, A. Girelli, A. Ragulskaya, S. Das, S. Berkowicz, M. Bin, M. Ladd-Parada, M. Filianina, H.-F. Poggemann, N. Begam, M. S. Akhundzadeh, S. Timmermann, L. Randolph, Y. Chushkin, T. Seydel, U. Boesenberg, J. Hallmann, J. Möller, A. Rodriguez-Fernandez, R. Rosca, R. Schaffer, M. Scholz, R. Shayduk, A. Zozulya, A. Madsen, F. Schreiber, F. Zhang, F. Perakis and C. Gutt, *Nat. Commun.*, 2022, **13**, 5528.
35 F. Otto, X. Sun, F. Schulz, C. Sanchez-Cano, N. Feliu, F. Westermeier and W. J. Parak, *Small*, 2022, **18**, 2201324.
36 K. Switalski, J. Fan, L. Li, M. Chu, E. Sarnello, P. Jemian, T. Li, Q. Wang and Q. Zhang, *J. Synchrotron Radiat.*, 2022, **29**, 1429–1435.
37 W. Jo, S. Stern, F. Westermeier, R. Rysov, M. Riepp, J. Schmehr, J. Lange, J. Becker, M. Sprung, T. Laurus, H. Graafsma, I. Lokteva, G. Grübel and W. Roseker, *Opt. Express*, 2023, **31**, 3315.
38 C. Caronna, Y. Chushkin, A. Madsen and A. Cupane, *Phys. Rev. Lett.*, 2008, **100**, 055702.
39 B. Ruta, Y. Chushkin, G. Monaco, L. Cipelletti, E. Pineda, P. Bruna, V. M. Giordano and M. Gonzalez-Silveira, *Phys. Rev. Lett.*, 2012, **109**, 165701.
40 F. Perakis, K. Amann-Winkel, F. Lehmkühler, M. Sprung, D. Mariedahl, J. A. Sellberg, H. Pathak, A. Späh, F. Cavalca, D. Schlesinger, A. Ricci, A. Jain, B. Massani, F. Aubree, C. J. Benmore, T. Loerting, G. Grübel, L. G. M. Pettersson and A. Nilsson, *Proc. Natl. Acad. Sci.*, 2017, **114**, 8193–8198.
41 F. Dallari, A. Martinelli, F. Caporaletti, M. Sprung, G. Grübel and G. Monaco, *Sci. Adv.*, 2020, **6**, aaz2982.
42 F. Lehmkühler, B. Hankiewicz, M. A. Schroer, L. Müller, B. Ruta, D. Sheyfer, M. Sprung, K. Tono, T. Katayama, M. Yabashi, T. Ishikawa, C. Gutt and G. Grübel, *Sci. Adv.*, 2020, **6**, eabc5916.
43 L. Frenzel, M. Dartsch, G. M. Balaguer, F. Westermeier, G. Grübel and F. Lehmkühler, *Phys. Rev. E*, 2021, **104**, L012602.
44 J. Li, M. Madhavi, S. Jeppson, L. Zhong, E. M. Dufresne, B. Aitken, S. Sen and R. Kukreja, *J. Phys. Chem. B*, 2022, **126**, 5320–5325.
45 F. Dallari, A. Martinelli, F. Caporaletti, M. Sprung, G. Baldi and G. Monaco, *Proc. Natl. Acad. Sci.*, 2023, **120**, e2213182120.
46 H. Guo, S. Ramakrishnan, J. L. Harden and R. L. Leheny, *J. Chem. Phys.*, 2011, **135**, 154903.
47 D. Orsi, L. Cristofolini, G. Baldi and A. Madsen, *Phys. Rev. Lett.*, 2012, **108**, 105701.
48 B. Ruta, O. Czakkel, Y. Chushkin, F. Pignon, R. Nervo, F. Zontone and M. Rinaudo, *Soft Matter*, 2014, **10**, 4547.
49 Q. Zhang, D. Bahadur, E. M. Dufresne, P. Grybos, P. Kmon, R. L. Leheny, P. Maj, S. Narayanan, R. Szczygiel, S. Ramakrishnan and A. Sandy, *Phys Rev Lett*, 2017, **119**, 178006.
50 D. Bahadur, Q. Zhang, E. M. Dufresne, P. Grybos, P. Kmon, R. L. Leheny, P. Maj, S. Narayanan, R. Szczygiel, J. W. Swan, A. Sandy and S. Ramakrishnan, *The Journal of Chemical Physics*, 2019, **151**, 104902.
51 L. Frenzel, I. Lokteva, M. Koof, S. Narayanan, G. Grübel and F. Lehmkühler, *ChemPhysChem*, 2020, **21**, 1318–1325.
52 E. B. Trigg, L. Wiegart, A. Fluerasu and H. Koerner, *Macro-*

molecules, 2021, **54**, 6575–6584.

53 Y. Xi, R. P. Murphy, Q. Zhang, A. Zemborain, S. Narayanan, J. Chae, S. Q. Choi, A. Fluerasu, L. Wiegart and Y. Liu, *Soft Matter*, 2023, **19**, 233–244.

54 A. Jain, F. Schulz, I. Lokteva, L. Frenzel, G. Grübel and F. Lehmkühler, *Soft Matter*, 2020, **16**, 2864–2872.

55 F. Schulz, T. Homolka, N. G. Bastús, V. Puntes, H. Weller and T. Vossmeyer, *Langmuir*, 2014, **30**, 10779–10784.

56 F. Schulz, G. T. Dahl, S. Besztejan, M. A. Schroer, F. Lehmkühler, G. Grübel, T. Vossmeyer and H. Lange, *Langmuir*, 2016, **32**, 7897–7907.

57 F. Schulz, J. Möller, F. Lehmkühler, A. J. Smith, T. Vossmeyer, H. Lange, G. Grübel and M. A. Schroer, *Particle & Particle Systems Characterization*, 2018, **35**, 1700319.

58 G. Grübel, A. Madsen and A. Robert, *Soft Matter Characterization*, Springer Netherlands, 2008, pp. 953–995.

59 A. R. Sandy, Q. Zhang and L. B. Lurio, *Ann. Rev. Mater. Res.*, 2018, **48**, 167–190.

60 A. Madsen, A. Fluerasu and B. Ruta, *Synchrotron Light Sources and Free-Electron Lasers*, Springer International Publishing, 2020, pp. 1989–2018.

61 A. Volk and C. J. Kähler, *Exp. Fluids*, 2018, **59**, 75.

62 R. Tian, G. Yang, H. Li, X. Gao, X. Liu, H. Zhu and Y. Tang, *Phys. Chem. Chem. Phys.*, 2014, **16**, 8828.

63 F. Ruffino, V. Torrisi and M. Grimaldi, *Physica E*, 2015, **74**, 388–399.

64 Q. Li, Y. Tang, X. He and H. Li, *AIP Adv.*, 2015, **5**, 107218.

65 A.-M. Philippe, D. Truzzolillo, J. Galvan-Myoshi, P. Dieudonné-George, V. Trappe, L. Berthier and L. Cipelletti, *Phys. Rev. E*, 2018, **97**, 040601.

66 V. Nigro, B. Ruzicka, B. Ruta, F. Zontone, M. Bertoldo, E. Buratti and R. Angelini, *Macromolecules*, 2020, **53**, 1596–1603.

67 K. Trachenko and A. Zaccone, *J. Phys.: Condens. Matter*, 2021, **33**, 315101.

68 L. Wang, G. Shan and P. Pan, *RSC Adv.*, 2014, **4**, 63513–63519.

69 O. Glatter and O. Kratky, *Small angle x-ray scattering*, Academic Press, 1982, p. 515.

70 N. Stribeck, *X-Ray Scattering of Soft Matter*, Springer, Berlin Heidelberg, 2007.

71 C. M. Jeffries, J. Ilavsky, A. Martel, S. Hinrichs, A. Meyer, J. S. Pedersen, A. V. Sokolova and D. I. Svergun, *Nature Reviews Methods Primers*, 2021, **1**, 70.

72 S. D. Vela, N. Begam, D. Dyachok, R. S. Schäufele, O. Matsarskaia, M. K. Braun, A. Girelli, A. Ragulskaya, A. Mariani, F. Zhang and F. Schreiber, *J. Phys. Chem. Lett.*, 2020, **11**, 7273–7278.

73 N. Begam, A. Ragulskaya, A. Girelli, H. Rahmann, S. Chandran, F. Westermeier, M. Reiser, M. Sprung, F. Zhang, C. Gutt and F. Schreiber, *Phys. Rev. Lett.*, 2021, **126**, 098001.

74 N. D. Anthuparambil, A. Girelli, S. Timmermann, M. Kowalski, M. S. Akhundzadeh, S. Retzbach, M. D. Senft, M. Dargasz, D. Gutmüller, A. Hiremath, M. Moron, Özgül Öztürk, H.-F. Poggemann, A. Ragulskaya, N. Begam, A. Tosson, M. Paulus, F. Westermeier, F. Zhang, M. Sprung, F. Schreiber and C. Gutt, *Nat. Commun.*, 2023, **14**, 5580.

75 J. Manson, D. Kumar, B. J. Meenan and D. Dixon, *Gold Bull.*, 2011, **44**, 99–105.

76 H. Abbasov, *ChemistrySelect*, 2023, **8**, e202301576.

77 D. Das Mahanta, D. R. Brown, S. Pezzotti, S. Han, G. Schwaab, M. S. Shell and M. Havenith, *Chem. Sci.*, 2023, **14**, 7381–7392.

78 A. M. Green, C. K. Ofosu, J. Kang, E. V. Anslyn, T. M. Truskett and D. J. Milliron, *Nano Lett.*, 2022, **22**, 1457–1466.

79 Z. M. Sherman, K. Kim, J. Kang, B. J. Roman, H. S. N. Crory, D. L. Conrad, S. A. Valenzuela, E. Lin, M. N. Dominguez, S. L. Gibbs, E. V. Anslyn, D. J. Milliron and T. M. Truskett, *Nano Lett.*, 2023, **23**, 3030–3037.

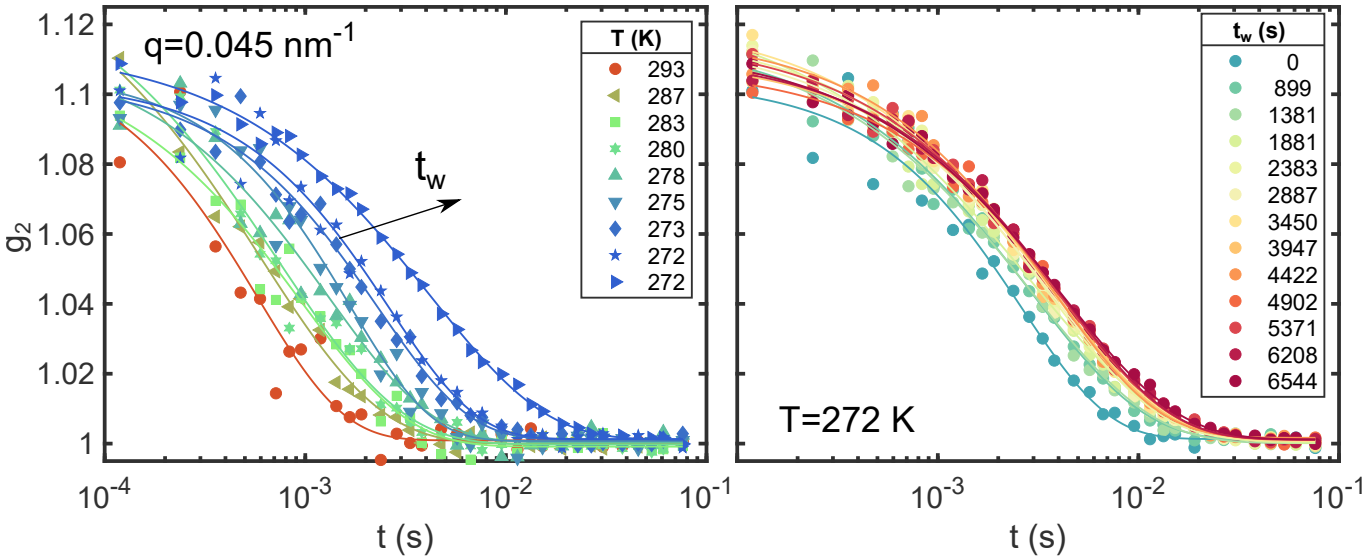

Fig. 1 Correlation functions g_2 at $q = 0.045$ nm^{-1} from run 2. In the left panel exemplary data is shown for different temperatures. At $T = 272$ K the first ($t_w = 0$ s) and last ($t_w = 6544$ s) measurement is shown. The right panel shows data at different t_w, all at $T = 272$ K. Lines are fits to Eq. 2.

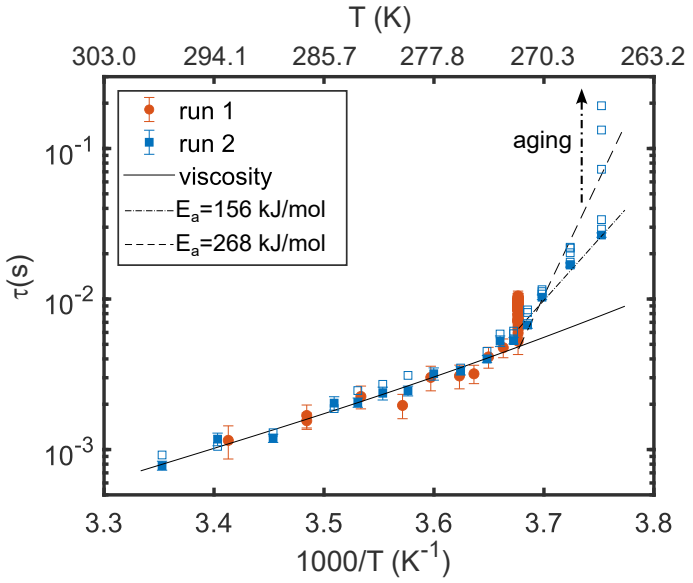

Fig. 2 Relaxation time τ as function of inverse temperature T^{-1} from both runs at $q = 0.045$ nm^{-1}. The filled squares for run 1 were measured directly after the target temperature has been reached, the open symbols were measured after waiting times up to typically 1500 s, the progress of t_w is indicated by the dot-dashed arrow. The data for run 2 at 272 K where measured continuously. The solid line represents the calculated relaxation time for diffusing particles of 14 nm radius, the dashed lines the fits to the Arrhenius laws for $T \leq 272$ K as described in the text.

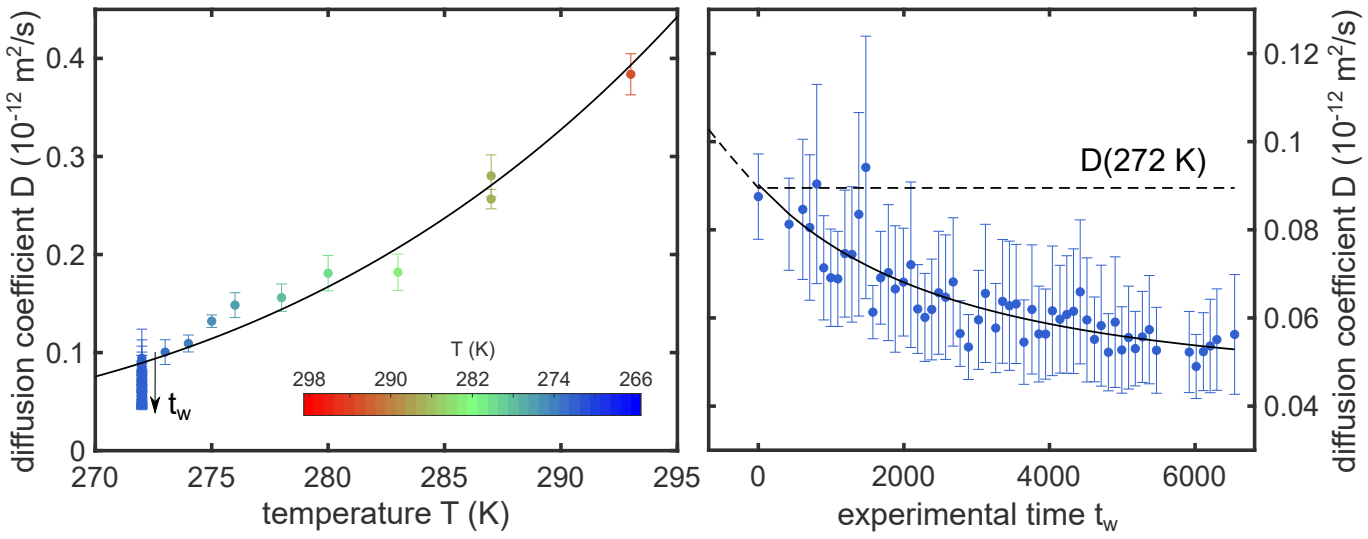

Fig. 3 Diffusion coefficients D for run 2. Left: D as function of temperature T. After reaching 272 K, D decreases with increasing experimental time t_w. Solid line is the calculation following Eq. 4. Right: D as function of t_w at 272 K. The decreasing D is empirically modelled by an power law resulting in $D \propto t_w^{-2}$ (purple line). The dashed line marks the expected diffusion constant at 272 K. In both panels the temperature is encoded in the color of the data points.

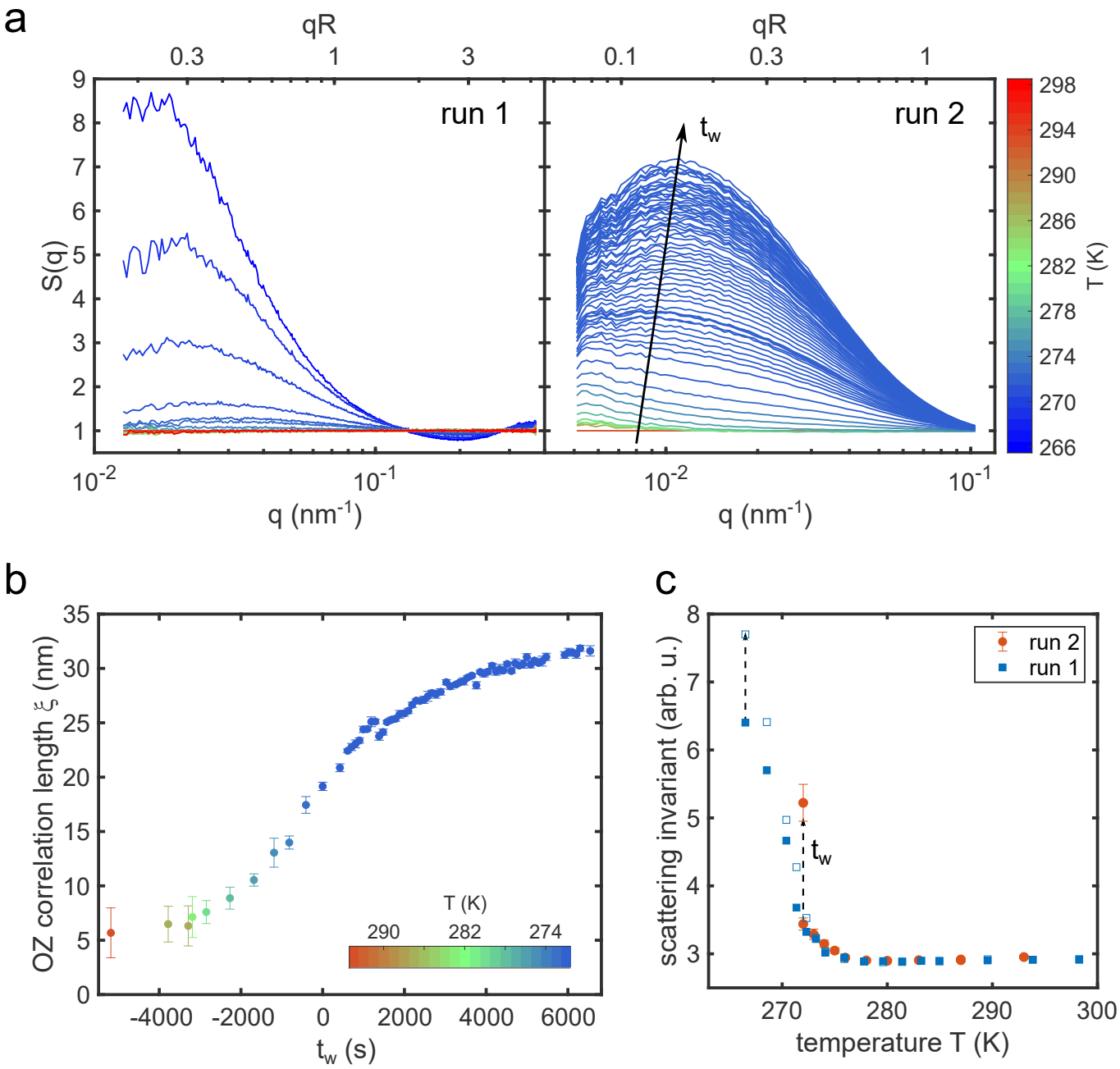

Fig. 4 (a) Structure factors $S(q)$ from both runs. The top axis is scaled by the particle radius $R = 14$ nm highlighting the low q-range studied. (b) Ornstein-Zernike correlation length ξ for the data from run 2. (c) Scattering invariant as function of temperature for both runs. The arrow shows the evolution with experimental time t_w. The color encodes the sample temperature as indicated by the colorbar in (a) and (b).

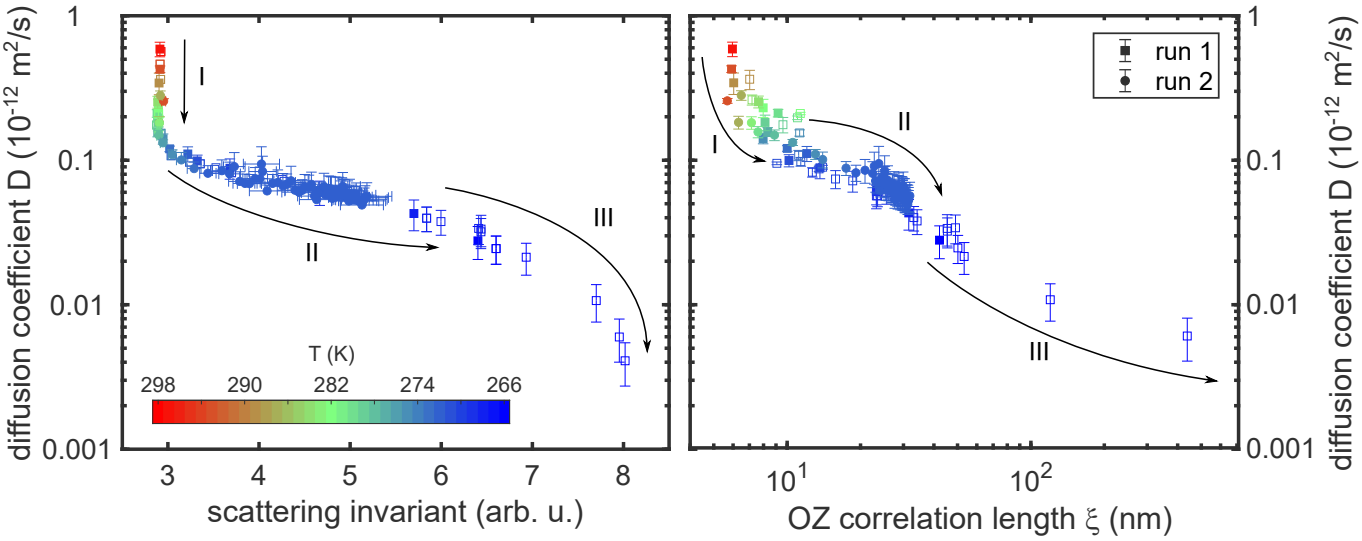

Fig. 5 Structure-dynamics correlation: diffusion coefficient D vs. the scattering invariant (left) and the Ornstein-Zernike correlation length ξ (right). The temperature is encoded by the color of the data points.